

Predictive control of blast furnace temperature in steelmaking with hybrid depth-infused quantum neural networks

Nayoung Lee

*POSCO Holdings Inc., 6261, Donghaean-ro, Nam-gu,
Pohang-si, Gyeongsangbuk-do, Republic of Korea*

Minsoo Shin

POSCO, 6261, Donghaean-ro, Nam-gu, Pohang-si, Gyeongsangbuk-do, Republic of Korea

Asel Sagingalieva, Ayush Joshi Tripathi, Karan Pinto, and Alexey Melnikov
Terra Quantum AG, Kornhausstrasse 25, 9000 St. Gallen, Switzerland

Accurate prediction and stabilization of blast furnace temperatures are crucial for optimizing the efficiency and productivity of steel production. Traditional methods often struggle with the complex and non-linear nature of the temperature fluctuations within blast furnaces. This paper proposes a novel approach that combines hybrid quantum machine learning with pulverized coal injection control to address these challenges. By integrating classical machine learning techniques with quantum computing algorithms, we aim to enhance predictive accuracy and achieve more stable temperature control. For this we utilized a unique prediction-based optimization method. Our method leverages quantum-enhanced feature space exploration and the robustness of classical regression models to forecast temperature variations and optimize pulverized coal injection values. Our results demonstrate a significant improvement in prediction accuracy over 25 percent and our solution improved temperature stability to ± 7.6 degrees of target range from the earlier variance of ± 50 degrees, highlighting the potential of hybrid quantum machine learning models in industrial steel production applications.

I. INTRODUCTION

Steel forms the backbone of the global economy, primarily due to its strength, durability, and versatility. Steel manufacturing is a highly complex and energy intensive endeavor. Steel production is a cornerstone of modern industry, and the blast furnace is at the heart of this process [1, 2]. In a blast furnace, raw materials such as iron ore, coke, and limestone are subjected to high temperatures to produce molten iron, which is then converted into steel [3–5]. Maintaining optimal temperature within these furnaces is critical for maximizing efficiency, reducing energy consumption, and ensuring high-quality output. The dynamic and highly non-linear nature of temperature variations within blast furnaces poses significant challenges to achieving stable and precise control [6].

One of the strategies employed to enhance the performance of blast furnaces is Pulverized Coal Injection (PCI), which involves injecting fine coal particles into the blast furnace to partially replace coke as a fuel and reducing agent. PCI offers numerous advantages, including cost reduction and improved control over the combustion process. However, effectively managing the injection rate and distribution of pulverized coal to maintain stable furnace temperatures requires sophisticated control strategies [7].

Machine learning models have demonstrated high performance in solving complex predictive problems in a wide range of domains [8], from economics [9–11] to energy [12] and industry [13, 14]. These problems are ad-

dressed by long short-term memory (LSTM) [15, 16] networks, which successfully model complex temporal patterns including: nonlinear interactions, long-term trends, seasonal and cyclical fluctuations.

Despite these advances, the performance of purely classical machine learning models may be constrained by factors such as limited or noisy datasets, high-dimensional inputs, and intricate fault dynamics [17, 18]. Recently, quantum computing has begun to transition from theoretical prototypes to early practical implementations, leveraging fundamental principles like entanglement and superposition to process information in ways that are difficult — or even impossible — for classical computers to mimic [19, 20]. This paradigm shift has spurred the development of quantum algorithms aimed at boosting performance in domains such as optimization, simulation, and cryptography, laying the groundwork for more specialized applications [21–23].

Within this emerging ecosystem, quantum machine learning (QML) has attracted considerable interest for its potential to handle complex problems that suffer from data scarcity or high-dimensional feature spaces [24–31]. QML models exploit high-dimensional Hilbert spaces to embed input features, enabling the representation of intricate correlations with fewer parameters compared to purely classical methods [32–35]. This capacity to map data into richer feature representations can offer significant advantages when dealing with nonstationary or noisy signals, as commonly encountered in industrial maintenance and prognostic settings [36, 37]. This paper explores the application of hybrid QML techniques to predict and stabilize blast furnace temperatures, fo-

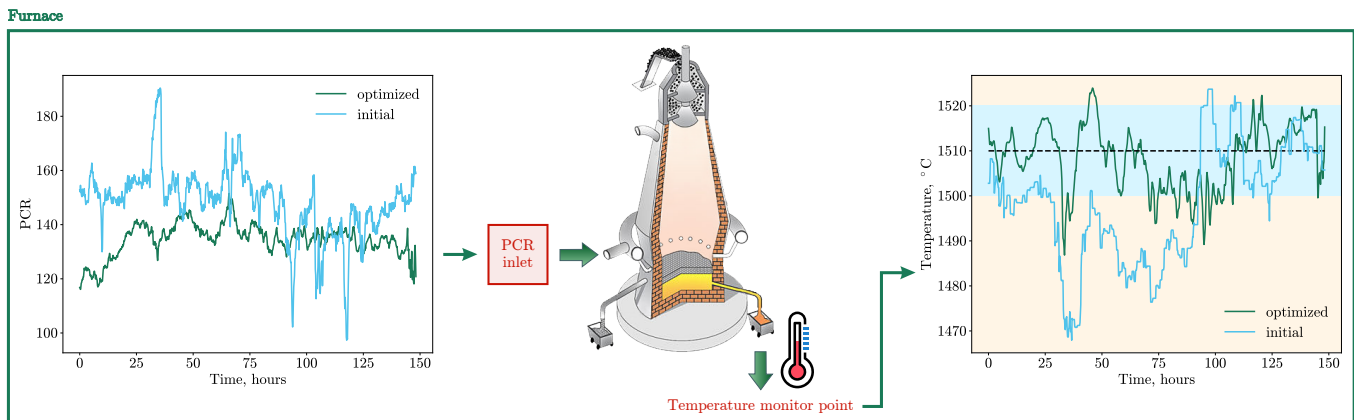


FIG. 1: Optimization of PCI policy and its effect on blast furnace temperature stabilization: the left plot shows a comparison between the original (initial) and optimized PCI injection rates over time, the right plot presents the resulting temperature trends: the optimized policy (green) successfully maintains the temperature within the target operational window (shaded blue area between 1500°C and 1510°C), while the initial policy (blue) leads to significant deviations and instability. Results were obtained using the hybrid machine learning models M_{all} and M_{optim} , following the procedure described in Algorithm 1 1.

cusing on optimizing PCI control parameters.

A practical approach to harnessing these quantum resources is through hybrid quantum-classical neural networks (HQNNs), which seamlessly combine both classical and quantum layers in a unified architecture [32, 38, 39]. In such models, quantum circuits often act as specialized components for data transformation or feature encoding, while the broader network structure — encompassing backpropagation, parameter updates, and other large-scale operations — remains anchored in conventional machine learning frameworks. This hybrid scheme exploits quantum effects in targeted segments of the computational pipeline, without sacrificing the scalability and reliability of well-established classical methods [40–43]. Early research suggests that HQNNs can achieve competitive or even superior performance compared with purely classical deep learning techniques, frequently demonstrating enhanced robustness against overfitting [44, 45].

Our approach integrates classical machine learning models with quantum algorithms to create a hybrid system capable of accurately forecasting temperature fluctuations and adjusting PCI settings in real-time. The proposed method leverages the unique capabilities of quantum computers to explore feature spaces more efficiently and solve optimization problems more effectively than traditional methods. By enhancing predictive accuracy and control stability, this QML approach, namely hybrid quantum neural network [46–48], holds the potential to significantly improve the efficiency and productivity of steel production.

A. Steel Making in Blast Furnace

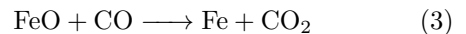
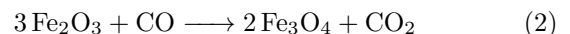
1. Process Overview

One of the key processes for producing iron is melting iron ore and through a reduction process, creating liquid iron [49]. This process of making hot metal is called the blast furnace process. The main reactions are as follows:

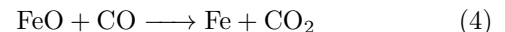
(1) Coke combustion: Coke (Carbon) and O_2 are oxidized at high temperatures to produce CO gas



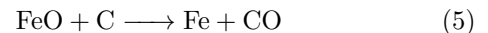
(2) Iron ore reduction: CO gas separates oxygen from iron ore to produce pure Fe



In the upper part of the furnace,



In the lower part,



The blast furnace process consists of raw material handling equipment, charging equipment, blast furnace main body, hot blast stove/air blower equipment, Pulverized Coal Injection equipment, burden and raw materials equipment, and gas cleaning equipment, and operates continuously 24 hours a day without stopping. The primary equipment in operation is the blast furnace main body, divided into five sections vertically. Starting from the top: Gas riser and rotating chute, the throat, the lumpy zone, the cohesive zone, where strong burden materials are dissolved and volume shrinks at the bosh, and

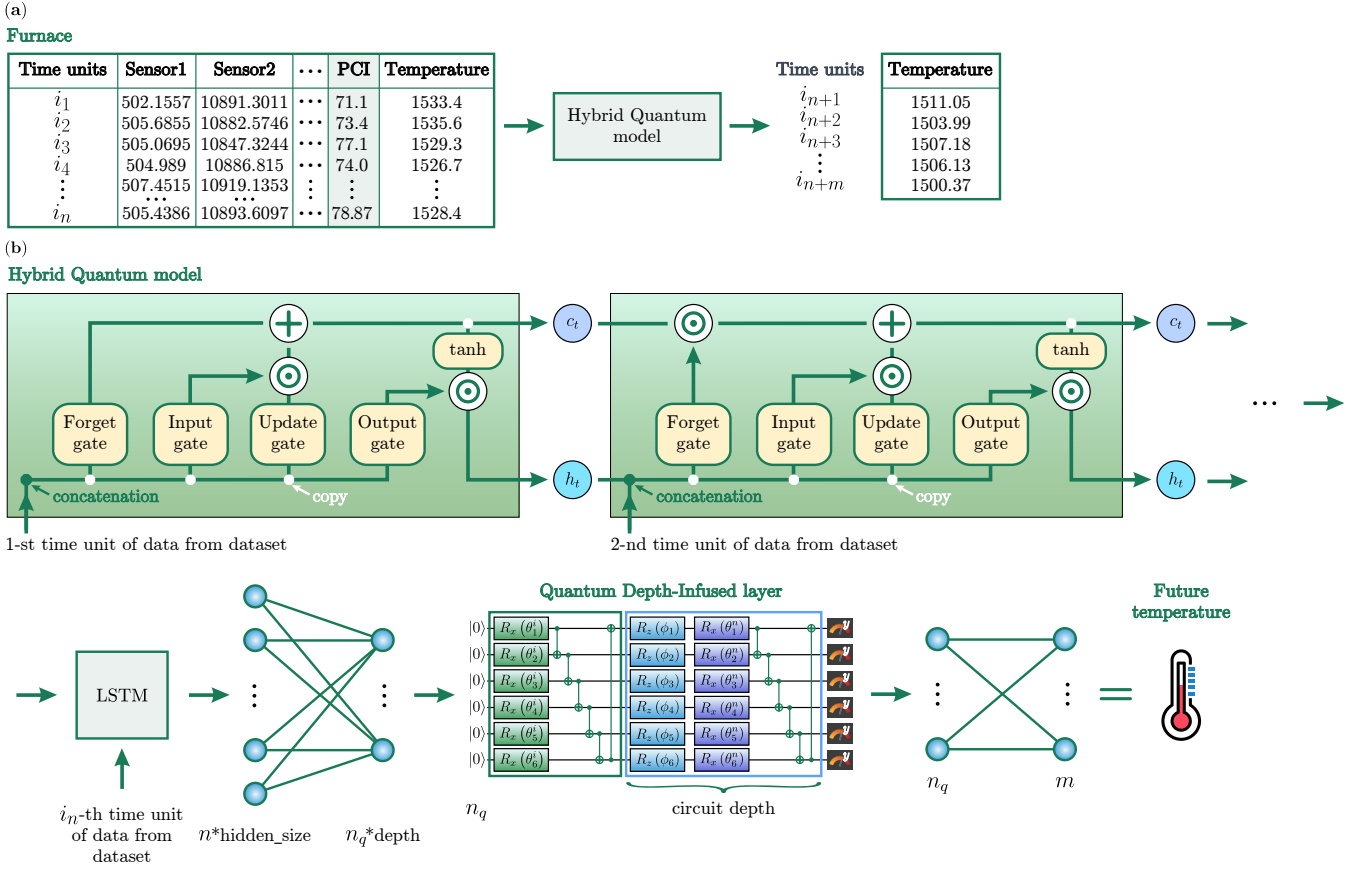


FIG. 2: Architecture of the Hybrid Quantum Model for Temperature Prediction in a Blast Furnace: (a) The input consists of time-series sensor data from the blast furnace, including PCI. The model predicts future temperatures based on this data. (b) The core of the model is a Hybrid Quantum Neural Network combining a classical LSTM network with a QDI layer. The LSTM processes temporal sequences, then passes its output through a fully connected layer. The intermediate representation is encoded into quantum states using the QDI layer, which applies rotation and entanglement gates over 6 qubits. A final fully connected layer maps the quantum-encoded features to the predicted future temperature values.

bottom, the wind tuyere is located where fuel combustion occurs and molten hot metal is stored at the hearth with the tap hole exit [50]. The point where the pulverized coal injection occurs is at the bottom of the blast furnace hearth. The tuyere applies heat to the mixture inside at a temperature of 1200°C and 4.0 bars.

PCI reduces the cost of raw material by substituting some of the high-cost coke with pulverized coal and medium oil injected into the blower at the bottom of the blast furnace [1, 51]. This involves inserting an injection lance into the internal duct of the tuyere at the bottom of the blast furnace for blowing.

2. Blast Furnace Temperature Prediction

In the iron making process, it is important to produce molten iron at a consistent temperature. Smooth iron making leads to stable subsequent processes. However, controlling the temperature consistently in the blast furnace is difficult due to factors such as the inability to see

inside, limited control points, and time delays between charging, control, and tapping [52–54].

The challenge of controlling the temperature originates from the delay between the control action and its effect, which cannot be clearly defined due to uncertainties in the relationship between them. Therefore, achieving stable temperature control requires understanding the relationship between the current control action and future temperature changes, which is not easy to predict accurately. To address this sub task, a sensor system that can provide a real-time information and analysis of temporal relationships among these sensors is needed, along with a model that can accurately predict the temperature.

Time delay characteristics are particularly problematic in the blast furnace operations. The blast furnace is large and inaccessible, making it impossible to track the materials inside or measure the high-temperature environment accurately. The lack of sensors that can withstand the extreme conditions of the blast furnace contributes to the inability to collect internal data. Time delays result from differences in transmission time, reaction time, and

spatial-temporal distributions within the smelting equipment. The difficulty in controlling the charging and tapping increases due to the uncertainty regarding how the top-charging modes affect operations and the quality of molten iron inside the blast furnace. According to field experts, the time delay between PCI charging and molten iron temperature is 2-3 hours.

Concerning changes in the ore type or interference from external factors can alter the normal operation point of the blast furnace, typically requiring experienced operators to adjust and transition to a new operating point based on their expertise. However, this subjective approach heavily relies on human intervention, leading to slow adaption and potentially enduring unstable furnace conditions. Unstable blast furnace conditions can cause fluctuations in molten iron composition, resulting in energy and resource wastage and diminished profitability. Therefore, analyzing and estimating the delay characteristics and parameters of the blast furnace process is crucial for modeling and optimal control of operating conditions and molten iron quality.

If the temperature drops too low and the iron ore fails to melt properly, there is a risk of blockages in the upper portion of the blast furnace. Conversely, if the temperature drops around the relatively lower tuyeres, the molten iron might solidify again, potentially causing the dangerous phenomenon known as "back lamination." In severe cases, explosions called "hang-ups" can occur, jeopardizing not only production but also the safety of workers near the blast furnace. Even within the range where iron ore melts, decreased temperatures can slow down the molten iron flow, leading to inconsistencies that may disrupt downstream production or result in internal blockages in the blast furnace.

Even just considering PCI, around 110 tons/hr (for one blast furnace) and 70 tons/hr (for other blast furnaces) are being used (currently costing 30-60 thousand won per ton). Achieving only about half of the target is possible if the operators are able to operate within a range of ± 15 degrees. To ensure that the operation stays within the safe temperature range, the target temperature is set higher. By stabilizing the hearth, i.e., controlling the molten iron temperature accurately, the target temperature can ultimately be lowered, thereby significantly reducing overall fuel usage.

B. Temperature Prediction and Control in the Blast furnace

Temperature prediction and control for the blast furnace has quite a long history. Prediction method is divided into mathematical model based methodology [55] and data driven methodology. Sometimes the silicon content are replacing the temperature since it is a good indicator and measuring the temperature of the molten iron is dangerous. Predicting the silicon content also divided into mathematical modeling [56, 57], and data-

driven methodologies [58–62].

To control the heat of a blast furnace, methods such as regulating the amount of input fuel and adjusting the air supply are available. Among these, for the primary purpose of stabilizing the furnace heat during sudden fluctuations, the control of the PCI rate is given priority. PCI consists of fine coal particles and is injected through the tuyeres.

The rate of pulverized coal injection is defined as :

$$\text{PCI (ton/hr)} = R_c - R_d \cdot P \cdot \frac{1000}{24}, \quad (6)$$

where R_c is corrected reductant rate, R_d is dropped coal rate and P is hot metal production from the blast furnace.

The amount of pulverized coal injection is calculated as part of the total reductant ratio (RAR) which is the sum of real time PCR and real time CR. This definition can be represented by the following :

$$\text{RAR} = \left(\frac{\text{PCI}_{\text{total}}}{P_{\text{real}}} \cdot 24 + \frac{C_c}{C_{pb}} \right) \cdot 1000, \quad (7)$$

where $\text{PCI}_{\text{total}}$ is total PCI rate, P_{real} is real time production, C_c is total coke house spt calculation, C_{pb} is pig production burden change.

The optimal amount of pulverized coal is determined based on how stably the furnace heat is controlled. Therefore, in order to predict the amount of pulverized coal that needs to be injected in the future, it is essential to first understand how the furnace heat will fluctuate in the future.

Molten Iron Temperature is measured by the operator at the tap hole once every 1-2 hours. Among these factors, the only direct measurement is the molten iron temperature, while the Si amount in molten iron is analyzed approximately 10 times a day through sampling. daily production, heat load, CO utilization, and H_2 utilization are values calculated based on other measured data.

In the past, to guide the optimal pulverized coal injection rate, a weighted linear sum calculation was performed for the 6 factors mentioned above. However, if only such a few factors are used for adjusting the pulverized coal injection rate, it becomes difficult to assert that the control reflects the current state of the blast furnace accurately. Therefore, using feature reduction techniques, the relationship between the molten iron temperature and other sensor data were used to perform the calculations.

II. RESULTS

A. Dataset

Data was obtained from a blast furnace in the POSCO's Gwangyang Steel Works, specifically from the

year 2023. Data has been recorded every minute and includes readings from approximately 580 sensors. These sensors measure variables such as tuyere velocity, CO gas utilization, H₂ gas utilization, stove temperature by position, hearth wall temperature by position, hot metal tapped temperature, cast speed, furnace top pressure, furnace gas temperature, stack pressure, air humidity, as well as the composition of pig iron and slag.

The presented data consist of two parts, each covering a time span of one month. These datasets contain 580 sensor columns, including PCI, as well as a Date column and four columns corresponding to temperature values at different tap holes of the furnace. The average of these four columns is considered as the temperature.

For the solution of the temperature time series prediction and its optimization problems, a feature engineering workflow has been proposed:

1. Data Selection, Treatment and Preprocessing
2. Data Dimensionality Reduction
3. Data Discretization

1. Dataset: Data Selection, Treatment and Pre-processing

To calculate the optimal amount of pulverized coal injection, the currently observed factors include daily iron production, heat load, CO utilization, H₂ utilization, Si amount in molten iron, and molten iron temperature. Daily iron production is the production volume calculated based on the amount of input fuel materials, and heat load is the load calculated using the cooling water flow rate, inlet temperature, and outlet temperature. CO Utilization is the gas utilization ratio calculated using the amounts of CO and CO₂ gases analyzed from the exhaust gas, while Si amount in molten iron is a value obtained through sampling and analysis of the hot metal in the laboratory.

To control the operation of a blast furnace, it is necessary to determine which of the temperature-related values to use as the target of control. The control points frequently used in blast furnaces in the past include flame temperature [63], Silicon content [59, 64, 65], hearth wall temperature [66], raceway temperature (upper gas temperature), hot metal temperature [67], and others. In this study, the molten iron temperature, frequently used at POSCO, was selected as the target. Regarding the location of molten iron temperature measurement, the measurement is performed at a point approximately 2 blocks away from the tap hole where the molten iron flows out of the furnace and passes through the runner. There are a total of 4 tap holes located in the cardinal directions of the circle, and the measurement interval starts about 100-120 minutes after the tap hole is opened, measuring once per hour with respect to the runner temperature on that side. This process is not automated, and individuals manually perform measurements using a temperature

sensor-equipped probing rod. Although there are efforts to automate the measurement equipment based on visual sensors at the tap hole, it has not been implemented yet due to ongoing stabilization issues. When selecting a representative temperature using this method, there are several issues to consider. Firstly, the molten iron temperature measurement period is not precise, and there is a time difference with other sensor data. Additionally, as the molten iron temperature is taken while passing through 2 blocks of the furnace, it is slightly cooler compared to the temperature inside the furnace. Furthermore, there are not just one but four molten iron temperatures. To set the representative value, any changes in values compared to the previous timestep are identified for all 4 sensors, and the updated value is considered as the representative temperature. In other words, when the temperature is freshly measured and updated, it is assumed to be most similar to the current runner temperature and updated accordingly. If there is no change, the previous value is copied and pasted to fill in the values between longer measurement intervals. As with typical outlier handling, missing values represented as 0 or null are handled, manual measurement error correction is performed where temperature values repeatedly measured within half the measurement period of the cycle are considered problematic and corrected by treating the last measured value as the correction for the previous erroneous measurement, and an additional IQR (Inter Quartile Range)-based error correction is applied as shown in Table I. In the case of IQR-based outlier correction, a distance of 5 IQR instead of the typical 1.5IQR distance between the 1st and 3rd quartiles is set, considering the data characteristics of the blast furnace operation.

TABLE I: IQR calculation for preprocessing of Molten Iron Temperature Measurement Data. For calculating the IQR, the minimum, median, maximum, Q1, and Q3 values were obtained for each sensor. When calculating the Anomaly Boundary using the IQR, it was observed that the standard 1.5 IQR did not match the anomaly range of the blast furnace, and thus it was adjusted to 5 IQR for anomaly value processing.

	Temp 1	Temp 2	Temp 3	Temp 4
Sample Size	47520	47520	47520	47520
Minimum	1301.832	1267.96	1208.67	1321.189
Q1	1500	1503.24	1502.87	1500
Median	1509.14	1521.06	1505.6	1510.83
Q3	1523.52	1525.05	1520.107	1521.98
Maximum	1589.26	1556.671	1556.854	1560.45
IQR (= Q1 - Q3)	23.52	21.81	17.23725	21.98
Q1 - 1.5 × IQR	1464.72	1470.525	1477.014	1467.03
Q3 + 1.5 × IQR	1558.8	1557.765	1545.963	1554.95
Q1 - 5 × IQR	1382.4	1385.64	1385.27	1382.4
Q3 + 5 × IQR	1617.6	1620.84	1620.47	1617.6

2. Dataset: Dimensionality Reduction

Due to the high-temperature characteristics of the blast furnace, it is not possible to visually inspect the internal state of the furnace or directly measure its state as pressure or temperature. Measurements can only be taken from the outermost wall just outside the innermost walls or from the flowing molten iron. This leads to the lack of indicators for furnace temperature will change means that only reactive measures are possible. If the operation is stable, reactive measures alone can maintain operation within a stable temperature range. However, in cases of unstable operation, even small variations in furnace temperature can have significant consequences. Generally, it takes about 6-8 hours for the iron and cokes charged at the top of the blast furnace to be discharged at the bottom. Therefore, it is challenging to control temperature fluctuations based on just one or two data points at a given time.

In this study, we utilized as diverse a range of sensor data as possible to identify sensors that can serve as indicators of temperature changes. Feature reduction techniques were used for extraction. Feature reduction is commonly used to reduce the number of input variables. By employing various methods to calculate relevance, the variables can be listed in order of their relevance or transformed into a smaller set of variables that are combinations of the original ones, as done in principal component analysis using linear projection. In this methodology, the former technique was used. This approach has the advantage of requiring the monitoring of fewer specific sensor values, making real-time computation more feasible. However, it has the disadvantage of reduced accuracy and sensitivity by ignoring sensor values with low influence.

The goal of this research is to develop an algorithm that can be practically applied to actual systems. Using a method involving gradient boosting, data-driven influence was calculated, which can be understood as the relevance to the targeted output variable. After calculating these influences, the top N sensors were selected based on their influence. The value of N is chosen arbitrarily, with an increase in number if the model results are biased or a decrease if the model is overfitting, has slow computation speed, or has too many model parameters.

To perform dimensionality reduction of sensors feature values, a gradient boosting (GB) model for feature importance estimation is proposed. Then feature extraction is conducted in two parts. In both GB models were trained on the first piece of datum, but in first part GB model is fitted to predict temperature value, and in the second is to predict PCI value. The relevant importance of the features was investigated according to decision-tree inside of in the boosting architecture [68].

Choosing all features with importance greater than one, 19 and 6 features for both part (respectively) were obtained. All those 25 feature are independent and appropriate for use (Table. II).

TABLE II: Influence (feature importance) on temperature using the gradient boosting for top 26 features. The order is ascending by influence. Corr is correlation on temperature.

No.	Influence	Corr
1	15.5603	-0.67
2	11.3173	-0.58
3	7.66	-0.44
4	7.3166	-0.11
5	5.8771	-0.43
6	5.6356	-0.26
7	4.6301	0.45
8	4.281	-0.46
9	3.8094	-0.38
10	3.7105	-0.18
11	3.6882	0.36
12	3.6216	0.1
13	3.3247	0.36
14	3.135	-0.05
15	2.8739	-0.53
16	2.5868	0.02
17	2.3724	0.13
18	2.3431	-0.05
19	1.751	-0.45
20	1.278	-0.18
21	1.0934	-0.51
22	0.7277	-0.03
23	0.6305	-0.38
24	0.4119	-0.37
25	0.2067	0.24
26	0.1572	0.31

3. Data: Discretization

Before discussion of the discretization, its necessity should be explained. As a final aim of the our work is to established an optimization relation between set PCI value and temperature, the values we change should have a magnitude, on what a change of PCI will lead to change of temperature. Thus, such discretization windows as 1hr, 10m and 20m were used (for comparison of optimization quality).

Discretization is performed as (e.g for temperature T) moving average:

$$T_{l_{\text{window}}}^{(t_0)} = \frac{1}{l_{\text{window}}} \sum_{t=t_0}^{t_0+l_{\text{window}}} T^{(t)}$$

and consequent shift on the length of the discretization period (l_{window}).

B. Building a model for temperature prediction

In order to calculate the optimal PCI values that satisfy the required temperature for steel production, it is first necessary to establish a relationship between the furnace temperature fluctuations resulting from changes in PCI. This leads to the problem of **temperature** prediction.

To solve the aforementioned prediction task, a special machine learning model M_T is developed. The main unit of this model is the LSTM [15, 69] layer, which consists of gates implementing the memory effect. In the proposed configuration, the LSTM layer with hidden size 143 encodes a 24-iterations of discretized sensors data vector of size 24×27 . After, it mapped to a future temperature vector of size 5×1 by a fully connected layer. Training is done by backpropagation of the L2 loss function between the predicted temperature vector and a real one.

To improve the achieved results, a hybridization of previous model was performed. As a result, such a hybrid quantum model was created (Fig. 2). Its structure differs slightly from the classical one, as a fully connected layer is divided into two, and a Quantum Depth-Infused (QDI) layer is added between new layers [70–73].

The QDI layer is used to expressively encode a large vector of size n into a small number of n_{qubits} that are available in the NISQ era. Its structure incorporates R_x , R_y rotations meant for angle embedding into quantum Hilbert space and CNOT operations for the entanglement.

$$R_y(\theta) = \begin{pmatrix} \cos\left(\frac{\theta}{2}\right) & -\sin\left(\frac{\theta}{2}\right) \\ \sin\left(\frac{\theta}{2}\right) & \cos\left(\frac{\theta}{2}\right) \end{pmatrix}$$

$$R_x(\theta) = \begin{pmatrix} \cos\left(\frac{\theta}{2}\right) & -i\sin\left(\frac{\theta}{2}\right) \\ -i\sin\left(\frac{\theta}{2}\right) & \cos\left(\frac{\theta}{2}\right) \end{pmatrix}$$

$$\text{CNOT} = \begin{pmatrix} 1 & 0 & 0 & 0 \\ 0 & 1 & 0 & 0 \\ 0 & 0 & 0 & 1 \\ 0 & 0 & 1 & 0 \end{pmatrix}$$

Implementation of QDI layer on Fig. 2 encodes data on $n_{qubits} = 6$ qubits through (green) R_x rotations with trainable weights and repetitive (blue) R_z data encoding rotations along with (purple) R_x trainable rotations, differing from one repetition to the another [74].

C. Building a model for all sensors prediction

Similar to the previous model, a model for predicting all 27 features of the dataset as the labels (M_{all}) is presented. Its structure is similar to the single label model (temperature), but with a larger hidden part of the LSTM and a MLP layer several times larger (the input is increased to $143 \times 24 \times 27$ versus 24×15). It's pipeline is similar to one described on Fig. 2: a short snippet of the dataset with size 27×24 is encoded into LSTM architecture, then output of LSTM goes through MLP layer and yields a vector of features 27×5 . Hybrid multi-feature models can be implemented by separating the MLP layers into two parts and adding a QDI layer in

between. However, creation of the hybrid model for all sensors predictions lays out of the scope of this work as training and optimizing hybrid quantum models is rather long process that requires high amount of compute resources. This approach can be considered as valuable in future findings.

D. Models evaluation

For evaluation of models prediction different approaches were used. Let's assume that in some time moment t , model predicts a temperatures vector $[T_{t+1}^{(t)}, T_{t+2}^{(t)}, T_{t+3}^{(t)}, T_{t+4}^{(t)}, T_{t+5}^{(t)}]$, where (t) - a last *real time moment* on that prediction based. If model predicts temperatures at $t + 1$, final vector $[T_{t+2}^{(t+1)}, T_{t+3}^{(t+1)}, T_{t+4}^{(t+1)}, T_{t+5}^{(t+1)}, T_{t+6}^{(t+1)}]$ overlaps with previous one. Depending on physical perspective, we can either average those vectors on their overlap, or use a specific vector for prediction, e.g: $[T_{t+i}^{(t)}, T_{t+1+i}^{(t+1)}, \dots]$. Fig. 4 shows a comparison of the LSTM and Hybrid Quantum LSTM models predictions.

The accuracy metrics used are RMSE and MAE, as shown below.

$$RMSE = \sqrt{\frac{1}{N} \sum_{t=1}^N (y^t - \hat{y}^t)^2} \quad (8)$$

$$MAE = \frac{1}{N} \sum_{t=1}^N |y^t - \hat{y}^t| \quad (9)$$

This model is designed to work on both classical and quantum computers using the same algorithm. At the moment, quantum processing units are still in the early stages of development [75]. Most available quantum computers are limited in size (typically fewer than 100 qubits), suffer from high error rates. Because of these limitations, running the model on classical hardware is currently faster and more accurate. However, as quantum hardware improves especially with advances in error correction and qubit scalability significant gains in speed and computational efficiency are expected. The key advantage of the current approach is that it prepares the model for a smooth transition to quantum platforms in the future, while still performing reliably on classical systems today.

E. Solving an optimization task

Finally, to solve the temperature optimization problem means to choose a specific optimization policy in terms of PCI values that, if set, will keep the temperature in the range of [1500 °C, 1510 °C].

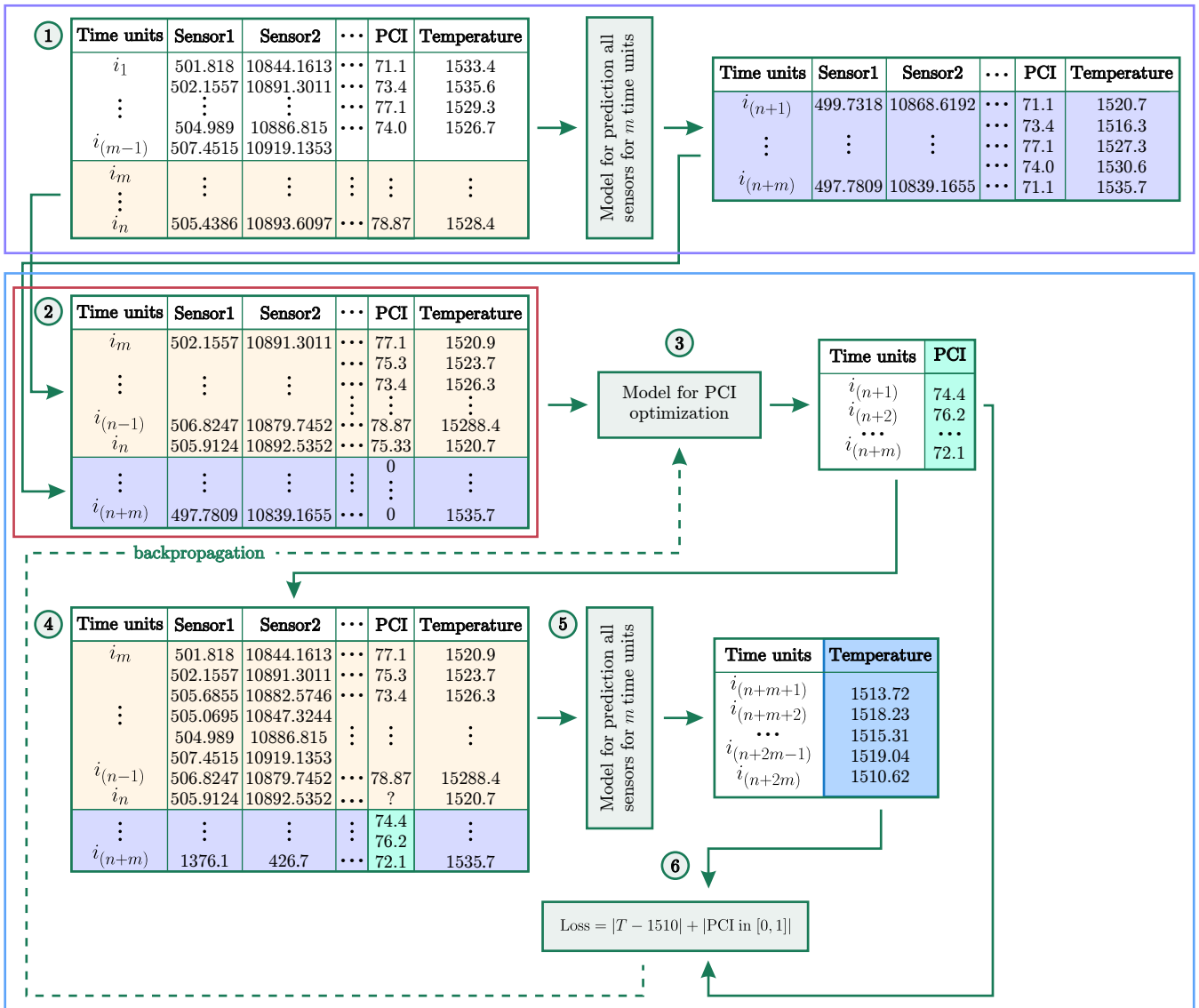


FIG. 3: Schematic representation of the optimization algorithm (Alg. 1). Step 1: predicting all features for 5 hours ahead using M_{all} . Step 2: concatenating predicted features with historical data and setting last m PCI values to 0. Step 3: predicting new PCI values for balancing temperature using M_{optim} . Step 4 and 5: predicting optimized temperature values. Step 6: calculating loss with respect to the optimized temperature and PCI values for training M_{optim} weights.

To find optimal PCI values, it's necessary to sort through all possible combinations of the values themselves and possible temperature values (predicted by previously developed models in case of the each optimization policy). Therefore, a gradient descent in the space of temperature PCI values is proposed as an optimization algorithm. It can be performed through an addition of the optimization model M_{optim} , which is implemented as an ordinary linear model in the presented pipeline.

The final algorithm, utilizes predictive capabilities of M_{all} model to establish connection between optimization policy and future temperature values and its graphical pipeline is shown in Fig. 3 and described step-by-step in Alg.1

Algorithm 1 Temperature-PCI optimization

1. On the i -th step of the algorithm, M_{all} model maps slice vector of features to the vector of future features prediction

$$M_{\text{all}} : \underbrace{\{\dots, \text{PCI}, T\}_{t=t_i}^{t=t_i+23}}_{\in \mathbb{R}^{24 \times 27}} \rightarrow \underbrace{\{\dots, \text{PCI}, T\}_{t=t_i+24}^{t=t_i+28}}_{\in \mathbb{R}^5 \times 27}$$

2. Then, truncated vector of features $\{\dots, \text{PCI}, T\}_{t=t_i+4}^{t=t_i+23}$ is combined with the predicted values $\{\dots, \text{PCI}, T\}_{t=t_i+24}^{t=t_i+28}$, but with $\{\text{PCI}\}_{t=t_i+24}^{t=t_i+28}$ policy set to zero $\{0\}_{t=t_i+24}^{t=t_i+28} \in \mathbb{R}^5$
3. M_{optim} model maps new vector of features to the vector of the possible optimization policy values (PCI values):

$$M_{\text{optim}} : \underbrace{\{\dots, \text{PCI}, T\}_{t=t_i+4}^{t=t_i+28}}_{\in \mathbb{R}^{24 \times 27}} \rightarrow \underbrace{\{\widehat{\text{PCI}}\}_{t=t_i+24}^{t=t_i+28}}_{\in \mathbb{R}^5}$$

- 4-5. To evaluate the quality of the optimization, M_{all} model maps new vector of features (with inclusion of the new PCI policy) to the vector of temperatures:

$$M_{\text{all}} : \underbrace{\{\dots, \text{PCI}, T\}_{t=t_i+4}^{t=t_i+28}}_{\in \mathbb{R}^{24 \times 27}} \rightarrow \underbrace{\{\widehat{T}\}_{t=t_i+29}^{t=t_i+33}}_{\in \mathbb{R}^5}$$

6. Finally, M_{optim} is tuned through the back-propagation of

$$\text{Loss} = \|\{\widehat{T}\}_{t=t_i+29}^{t=t_i+33} - 1510\|_1 + \underbrace{\|\{\widehat{\text{PCI}}\}_{t=t_i+24}^{t=t_i+28}\|_1}_{\text{regularization term}} \in [0, 1]$$

F. Training

As described above, models M_T and M_{all} were trained on the entire dataset. The input data was divided into training and test subsets in an 8:2 ratio. The training data was scaled using the MinMax scaling technique. The RMSE loss function was employed during the weight optimization process.

The parameters of the classical layers were optimized using the backpropagation [76] algorithm, accessed automatically within the PyTorch [77] library. This algorithm was used to compute the gradients of the loss function with respect to the network parameters, facilitating optimization via gradient descent. However, the inclusion of the QDI layer in the M_T model complicates optimization. To address the quantum gradient computation challenge, we employ the PennyLane [78] framework, which provides various optimization techniques, utilizing adjoint differentiation. This method effectively optimizes the variational parameters of the quantum layers, completing our training pipeline.

After training model M_{all} , the focus shifts to the PCI stabilization model M_{optim} as per the algorithm outlined in Section III E. A key detail is that during this phase, the weights of model M_{all} were frozen and not subject to optimization. As this model lacks quantum components, classical optimization algorithms were successfully

applied during this training.

G. Results

To analyze time-series correlations, a machine learning-based model called GB was used. This is an ensemble technique that combines multiple models to create a better model and is based on tree models. By performing GB, the influence of each variable on the final output can be calculated, which differs from simple distance-based correlation values. This analysis classifies the entire time-series data, including the time lagged results. The analysis identified the following highly correlated sensors as shown in the table below: targeted PCI rate, hearth wall temperatures (8 sensors), elemental composition in SLAG (TiO_2 , MnO , S , SiO_2), average charging time, STAVE temperatures (3 sensors), cooling plate temperatures (2 sensors), stack average temperature, real-time CR, BOSH gas volume, real-time FR, PCR, flame temperature, and OBYC.

From the results, a notable difference is observed between the values derived from influence calculation and those from simple correlation analysis, along with variations in rankings. Additionally, the influence-based time-series correlation analysis identified variables that were not previously well-monitored, such as SLAG TiO_2 , SLAG MnO , SLAG S , and ObyC, thus making use of high-information-value data that had not been utilized effectively.

In the furnace temperature prediction model, the accuracy significantly improved when comparing the conventional AI model to the hybrid quantum model. Also The size of the AI model was reduced compared to the conventional AI model. A reduction in the total number of training parameters and parameter size is evident.

III. CONCLUSION

In this work, we introduced a complete machine learning pipeline, consisting of sophisticated data preprocessing and models selection for concrete description of the inner processes of the blast furnace, thus solving the temperature prediction problem. On that basis, a ML-driven optimization approach for PCI injection rate optimization is proposed.

The implemented models, including hybrid quantum ones incorporating QDI layer, are able to predict temperature or all sensor data with high accuracy: 4.46 RMSE (for quantum temperature model in 1 hour prediction) and 8.33 RMSE (for classical model respectively). Here, quantum machine learning model shows its superior results over ML model without quantum layer with maximum of 25 % accuracy.

Invented predictive models lay the foundation for accurate temperature control, which is proposed to be implemented via an optimizer model (Alg. 1). Using simple

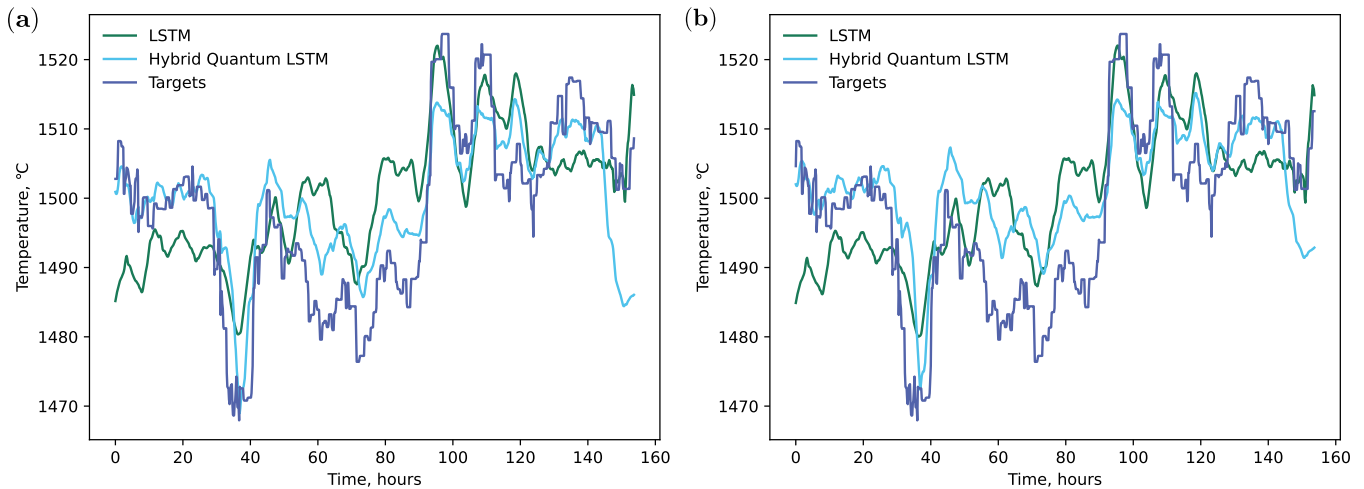


FIG. 4: Comparison of the temperature predictions between the LSTM and Hybrid Quantum LSTM models. (a) Predictions are made for 10 minutes forward (1 timestamp). Hybrid model outperforms the classical one with $RMSE_q = 7.59$ and $RMSE_{cl} = 9.98$. (b). Predictions are made for 50 minutes forward (5 timestamps). Hybrid model outperforms the classical one with $RMSE_q = 8.55$ and $RMSE_{cl} = 9.91$.

linear regression as an optimizer, the temperature was controlled within half of the required range with an accuracy of 7.6°C , successfully satisfying requirements of the steel production.

Achieved results, both in terms of temperature prediction and PCI policy optimization outstand contemporary industrial results, thus paving the way for quantum machine learning application in real life and industry problems.

IV. DISCUSSION

With sufficient iterative computation, it was possible to derive guidance values that reduce post-control tem-

perature fluctuations to within 7.6°C (Fig. 1). However, to operate the model in real-time, the number of possible iterations (due to the time latency of the system) is limited, so it is necessary to cap the iteration count. Therefore, future experiments should be carried out by varying the number of regression iterations and prediction steps to assess accuracy within a practically usable number of iterations.

-
- [1] Anne M Carpenter. Use of PCI in blast furnaces. IEA Clean Coal Centre London, UK, 2006.
 - [2] Zhuang-nian Li, Man-sheng Chu, Zheng-gen Liu, Gen-ji Ruan, and Bao-feng Li. Furnace heat prediction and control model and its application to large blast furnace. High Temperature Materials and Processes, 38(2019):884–891, 2019.
 - [3] Dewen Jiang, Zhenyang Wang, Kejiang Li, Jianliang Zhang, and Song Zhang. Machine learning models for predicting and controlling the pressure difference of blast furnace. JOM, 75(11):4550–4561, 2023.
 - [4] Song Zhang, Dewen Jiang, Zhenyang Wang, Fei Wang, Jianliang Zhang, Yanbing Zong, and Shuigen Zeng. Predictive modeling of the hot metal sulfur content in a blast furnace based on machine learning. Metals, 13(2):288, 2023.
 - [5] Ricardo A Calix, Orlando Ugarte, Tyamo Okosun, and Hong Wang. Machine learning-based regression models for ironmaking blast furnace automation. Dynamics, 3(4):636–655, 2023.
 - [6] Hong-Wei Xu, Wei Qin, Yan-Ning Sun, You-Long Lv, and Jie Zhang. Attention mechanism-based deep learning for heat load prediction in blast furnace ironmaking process. Journal of Intelligent Manufacturing, 35(3):1207–1220, 2024.
 - [7] Meng Yuan, Ping Zhou, Ming-liang Li, Rui-feng Li, Hong Wang, and Tian-you Chai. Intelligent multivariable modeling of blast furnace molten iron quality based on dynamic AGA-ANN and PCA. Journal of Iron and Steel Research International, 22(6):487–495, 2015.
 - [8] Mario Krenn, Jonas Landgraf, Thomas Foessel, and Florian Marquardt. Artificial intelligence and machine learning for quantum technologies. Physical Review A, 107(1):010101, 2023.
 - [9] James H Stock and Mark W Watson. Forecasting with many predictors. Handbook of economic forecasting,

- 1:515–554, 2006.
- [10] Eric Paquet and Farzan Soleymani. QuantumLeap: Hybrid quantum neural network for financial predictions. *Expert Systems with Applications*, 195:116583, 2022.
- [11] Kimleang Kea, Dongmin Kim, Chansreynich Huot, Tae-Kyung Kim, and Youngsun Han. A hybrid quantum-classical model for stock price prediction using quantum-enhanced long short-term memory. *Entropy*, 26(11):954, 2024.
- [12] Nan Feng and Conglin Ran. Design and optimization of distributed energy management system based on edge computing and machine learning. *Energy Informatics*, 8(1):17, 2025.
- [13] Alessandro Sebastianelli, Daniela Alessandra Zaidenberg, Dario Spiller, Bertrand Le Saux, and Silvia Liberata Ullo. On circuit-based hybrid quantum neural networks for remote sensing imagery classification. *IEEE Journal of Selected Topics in Applied Earth Observations and Remote Sensing*, 15:565–580, 2021.
- [14] Keeyoung Kim, Byeongrak Seo, Sang-Hoon Rhee, Seungmoon Lee, and Simon S Woo. Deep learning for blast furnaces: Skip-dense layers deep learning model to predict the remaining time to close tap-holes for blast furnaces. In *Proceedings of the 28th ACM international conference on information and knowledge management*, pages 2733–2741, 2019.
- [15] Sepp Hochreiter and Jürgen Schmidhuber. Long short-term memory. *Neural computation*, 9(8):1735–1780, 1997.
- [16] Felix A Gers, Jürgen Schmidhuber, and Fred Cummins. Learning to forget: Continual prediction with lstm. *Neural computation*, 12(10):2451–2471, 2000.
- [17] Christopher M Bishop. *Pattern recognition and machine learning (information science and statistics)*. Springer New York, 2007.
- [18] Ian Goodfellow, Yoshua Bengio, Aaron Courville, and Yoshua Bengio. *Deep learning*, volume 1. MIT press Cambridge, 2016.
- [19] Michael A Nielsen and Isaac L Chuang. *Quantum computation and quantum information*. Cambridge university press, 2010.
- [20] Jacob Biamonte, Peter Wittek, Nicola Pancotti, Patrick Rebentrost, Nathan Wiebe, and Seth Lloyd. Quantum machine learning. *Nature*, 549(7671):195–202, 2017.
- [21] Ashley Montanaro. Quantum algorithms: an overview. *npj Quantum Information*, 2(1):1–8, 2016.
- [22] John Preskill. Quantum computing in the NISQ era and beyond. *Quantum*, 2:79, 2018.
- [23] Arunava Majumder, Marius Krumm, Tina Radkohl, Lukas J Fiderer, Hendrik Poulsen Nautrup, Sofiene Jerbi, and Hans J Briegel. Variational measurement-based quantum computation for generative modeling. *Physical Review A*, 110(6):062616, 2024.
- [24] Patrick Rebentrost, Masoud Mohseni, and Seth Lloyd. Quantum support vector machine for big data classification. *Physical review letters*, 113(13):130503, 2014.
- [25] Carlo Ciliberto, Mark Herbster, Alessandro Davide Ialongo, Massimiliano Pontil, Andrea Rocchetto, Simone Severini, and Leonard Wossnig. Quantum machine learning: a classical perspective. *Proceedings of the Royal Society A: Mathematical, Physical and Engineering Sciences*, 474(2209):20170551, 2018.
- [26] Maria Schuld and Francesco Petruccione. Supervised learning with quantum computers. *Quantum science and technology (Springer, 2018)*, 2018.
- [27] Yudong Cao, Gian Giacomo Guerreschi, and Alán Aspuru-Guzik. Quantum neuron: an elementary building block for machine learning on quantum computers. *arXiv preprint arXiv:1711.11240*, 2017.
- [28] Iordanis Kerenidis, Jonas Landman, and Anupam Prakash. Quantum algorithms for deep convolutional neural networks. *arXiv preprint arXiv:1911.01117*, 2019.
- [29] Iordanis Kerenidis, Jonas Landman, Alessandro Luongo, and Anupam Prakash. q-means: A quantum algorithm for unsupervised machine learning. *Advances in neural information processing systems*, 32, 2019.
- [30] Anna Dawid, Julian Arnold, Borja Requena, Alexander Gresch, Marcin Plodzień, Kaelan Donatella, Kim A Nicoli, Paolo Stornati, Rouven Koch, Miriam Büttner, et al. Modern applications of machine learning in quantum sciences. *arXiv preprint arXiv:2204.04198*, 2022.
- [31] Fulvio Flamini, Marius Krumm, Lukas J Fiderer, Thomas Müller, and Hans J Briegel. Towards interpretable quantum machine learning via single-photon quantum walks. *Quantum Science and Technology*, 9(4):045011, 2024.
- [32] Vojtěch Havlíček, Antonio D Córcoles, Kristan Temme, Aram W Harrow, Abhinav Kandala, Jerry M Chow, and Jay M Gambetta. Supervised learning with quantum-enhanced feature spaces. *Nature*, 567(7747):209–212, 2019.
- [33] Maria Schuld and Nathan Killoran. Quantum machine learning in feature hilbert spaces. *Physical review letters*, 122(4):040504, 2019.
- [34] Alexandr Sedykh, Maninadh Podapaka, Asel Saginalieva, Karan Pinto, Markus Pfitsch, and Alexey Melnikov. Hybrid quantum physics-informed neural networks for simulating computational fluid dynamics in complex shapes. *Machine Learning: Science and Technology*, 5(2):025045, 2024.
- [35] Arsenii Senokosov, Alexandr Sedykh, Asel Saginalieva, Basil Kyriacou, and Alexey Melnikov. Quantum machine learning for image classification. *Machine Learning: Science and Technology*, 5(1):015040, 2024.
- [36] Asel Saginalieva, Stefan Komorniyk, Arsenii Senokosov, Ayush Joshi, Alexander Sedykh, Christopher Mansell, Olga Tsurkan, Karan Pinto, Markus Pfitsch, and Alexey Melnikov. Photovoltaic power forecasting using quantum machine learning. *arXiv preprint arXiv:2312.16379*, 2023.
- [37] Dimitrios Emmanoulopoulos and Sofija Dimoska. Quantum machine learning in finance: Time series forecasting. *arXiv preprint arXiv:2202.00599*, 2022.
- [38] Lukas Bischof, Stefan Teodoropol, Rudolf M Fuchsln, and Kurt Stockinger. Hybrid quantum neural networks show strongly reduced need for free parameters in entity matching. *Scientific Reports*, 15(1):4318, 2025.
- [39] Yuchen Sun, Dongfen Li, Qiuyu Xiang, Yuhang Yuan, Zhikang Hu, Xiaoyu Hua, Yangyang Jiang, Yonghao Zhu, and You Fu. Scalable quantum convolutional neural network for image classification. *Physical A: Statistical Mechanics and its Applications*, 657:130–226, 2025.
- [40] Michael Broughton, Guillaume Verdon, Trevor McCourt, Antonio J Martinez, Jae Hyeon Yoo, Sergei V Isakov, Philip Massey, Ramin Halavati, Murphy Yuezhen Niu, Alexander Zlokapa, et al. Tensorflow quantum: A software framework for quantum machine learning. *arXiv preprint arXiv:2003.02989*, 2020.
- [41] Jonas Landman, Natansh Mathur, Yun Yvonna Li, Mar-

- tin Strahm, Skander Kazdaghi, Anupam Prakash, and Iordanis Kerenidis. Quantum methods for neural networks and application to medical image classification. *Quantum*, 6:881, 2022.
- [42] Asel Sagingalieva, Andrii Kurkin, Artem Melnikov, Daniil Kuhmistrov, et al. Hybrid quantum ResNet for car classification and its hyperparameter optimization. *Quantum Machine Intelligence*, 5(2):38, 2023.
- [43] Tatjana Protasevich, Mikhail Surmach, Aleksandr Sedykh, Olga Tsurkan, Matvei Anoshin, Vadim Lopatkin, and Leonid Fedichkin. Multi-stream physics hybrid networks for solving navier-stokes equations. *arXiv preprint arXiv:2504.01891*, 2025.
- [44] Amira Abbas, David Sutter, Christa Zoufal, Aurélien Lucchi, Alessio Figalli, and Stefan Woerner. The power of quantum neural networks. *Nature Computational Science*, 1(6):403–409, 2021.
- [45] Julian Berberich, Daniel Fink, Daniel Pranjic, Christian Tutschku, and Christian Holm. Training robust and generalizable quantum models. *Physical Review Research*, 6(4):043326, 2024.
- [46] Marcello Benedetti, Erika Lloyd, Stefan Sack, and Mattia Fiorentini. Parameterized quantum circuits as machine learning models. *Quantum science and technology*, 4(4):043001, 2019.
- [47] Amira Abbas, David Sutter, Christa Zoufal, Aurélien Lucchi, Alessio Figalli, and Stefan Woerner. The power of quantum neural networks. *Nature Computational Science*, 1(6):403–409, 2021.
- [48] Andrea Skolik, Jarrod R McClean, Masoud Mohseni, Patrick Van Der Smagt, and Martin Leib. Layerwise learning for quantum neural networks. *Quantum Machine Intelligence*, 3:1–11, 2021.
- [49] Maarten Geerdes, Renard Chaigneau, and Oscar Lingardi. *Modern blast furnace ironmaking: an introduction (2020)*. Ios Press, 2020.
- [50] A Agarwal, U Tewary, F Pettersson, S Das, Henrik Saxen, and Nirupam Chakraborti. Analysing blast furnace data using evolutionary neural network and multi-objective genetic algorithms. *Ironmaking & Steelmaking*, 37(5):353–359, 2010.
- [51] Bo Zhou, Hao Ye, Haifeng Zhang, and Mingliang Li. Process monitoring of iron-making process in a blast furnace with PCA-based methods. *Control engineering practice*, 47:1–14, 2016.
- [52] Ping Zhou, Meng Yuan, Hong Wang, Zhuo Wang, and Tian-You Chai. Multivariable dynamic modeling for molten iron quality using online sequential random vector functional-link networks with self-feedback connections. *Information Sciences*, 325:237–255, 2015.
- [53] Xinmin Zhang, Manabu Kano, and Shinroku Matsuzaki. A comparative study of deep and shallow predictive techniques for hot metal temperature prediction in blast furnace ironmaking. *Computers & chemical engineering*, 130:106575, 2019.
- [54] Tathagata Bhattacharya. Prediction of silicon content in blast furnace hot metal using partial least squares (PLS). *ISIJ international*, 45(12):1943–1945, 2005.
- [55] Mansheng Chu, Jun-ichiro Yagi, and Fengman Shen. *Modelling on blast furnace process and innovative ironmaking technologies*. Northeastern University Press, 2006.
- [56] Henrik Saxén and Frank Pettersson. Nonlinear prediction of the hot metal silicon content in the blast furnace. *ISIJ international*, 47(12):1732–1737, 2007.
- [57] Antti Nurkkala, Frank Pettersson, and Henrik Saxen. Nonlinear modeling method applied to prediction of hot metal silicon in the ironmaking blast furnace. *Industrial & Engineering Chemistry Research*, 50(15):9236–9248, 2011.
- [58] Dong Qiu, De-Jiang Zhang, Wen You, Niao-Na Zhang, and Hui Li. An application of prediction model in blast furnace hot metal silicon content based on neural network. In *2009 International Conference on Apperceiving Computing and Intelligence Analysis*, pages 61–64. IEEE, 2009.
- [59] Henrik Saxen, Chuanhou Gao, and Zhiwei Gao. Data-driven time discrete models for dynamic prediction of the hot metal silicon content in the blast furnace—A review. *IEEE Transactions on Industrial Informatics*, 9(4):2213–2225, 2012.
- [60] Haigang Zhang, Sen Zhang, Yixin Yin, and Xianzhong Chen. Prediction of the hot metal silicon content in blast furnace based on extreme learning machine. *International Journal of Machine Learning and Cybernetics*, 9:1697–1706, 2018.
- [61] Wei Chen, Fanbei Kong, Baoxiang Wang, and Yuhan Li. Application of grey relational analysis and extreme learning machine method for predicting silicon content of molten iron in blast furnace. *Ironmaking & Steelmaking*, 46(10):974–979, 2019.
- [62] Dewen Jiang, Xinfu Zhou, Zhenyang Wang, Kejiang Li, and Jianliang Zhang. Predictive modeling of the hot metal silicon content in blast furnace based on ensemble method. *Metallurgical Research & Technology*, 119(5):515, 2022.
- [63] Yasin Tunckaya and Etem Köklükaya. Comparative performance evaluation of blast furnace flame temperature prediction using artificial intelligence and statistical methods. *Turkish Journal of Electrical Engineering and Computer Sciences*, 24(3):1163–1175, 2016.
- [64] Heng Zhou, Haifeng Zhang, Chunjie Yang, and Youxian Sun. Deep learning based silicon content estimation in ironmaking process. *IFAC-PapersOnLine*, 53(2):10737–10742, 2020.
- [65] Jian Chen. A predictive system for blast furnaces by integrating a neural network with qualitative analysis. *Engineering Applications of Artificial Intelligence*, 14(1):77–85, 2001.
- [66] Kexin Jiao, Jianliang Zhang, Qinfu Hou, Zhengjian Liu, and Guangwei Wang. Analysis of the relationship between productivity and hearth wall temperature of a commercial blast furnace and model prediction. *steel research international*, 88(9):1600475, 2017.
- [67] Xinmin Zhang, Manabu Kano, and Shinroku Matsuzaki. Ensemble pattern trees for predicting hot metal temperature in blast furnace. *Computers & Chemical Engineering*, 121:442–449, 2019.
- [68] Anna Veronika Dorogush, Vasily Ershov, and Andrey Gulin. Catboost: gradient boosting with categorical features support. *arXiv preprint arXiv:1810.11363*, 2018.
- [69] Hui-Xin Tian, Dai-Xu Ren, and Kun Li. A hybrid vibration signal prediction model using autocorrelation local characteristic-scale decomposition and improved long short term memory. *IEEE Access*, 7:60995–61007, 2019.
- [70] Asel Sagingalieva, Mohammad Kordzanganeh, Nurbolat Kenbayev, Daria Kosichkina, Tatiana Tomashuk, and Alexey Melnikov. Hybrid quantum neural network for

- drug response prediction. *Cancers*, 15(10):2705, 2023.
- [71] Matvei Anoshin, Asel Sagingalieva, Christopher Mansell, Dmitry Zhiganov, Vishal Shete, Markus Pflitsch, and Alexey Melnikov. Hybrid quantum cycle generative adversarial network for small molecule generation. *IEEE Transactions on Quantum Engineering*, 5:2500514, 2024.
- [72] Luca Lusnig, Asel Sagingalieva, Mikhail Surmach, Tatjana Protasevich, Ovidiu Michiu, Joseph McLoughlin, Christopher Mansell, Graziano de’Petris, Deborah Bonazza, Fabrizio Zanconati, et al. Hybrid quantum image classification and federated learning for hepatic steatosis diagnosis. *Diagnostics*, 14(5):558, 2024.
- [73] Maniraman Periyasamy, Nico Meyer, Christian Ufrecht, Daniel D Scherer, Axel Plinge, and Christopher Mutschler. Incremental data-uploading for full-quantum classification. In *2022 IEEE International Conference on Quantum Computing and Engineering (QCE)*, pages 31–37. IEEE, 2022.
- [74] Mo Kordzanganeh, Pavel Sekatski, Leonid Fedichkin, and Alexey Melnikov. An exponentially-growing family of universal quantum circuits. *Machine Learning: Science and Technology*, 4(3):035036, 2023.
- [75] Mohammad Kordzanganeh, Markus Buchberger, Basil Kyriacou, Maxim Povolotskii, Wilhelm Fischer, Andrii Kurkin, Wilfrid Somogyi, Asel Sagingalieva, Markus Pflitsch, and Alexey Melnikov. Benchmarking simulated and physical quantum processing units using quantum and hybrid algorithms. *Advanced Quantum Technologies*, 6(8):2300043, 2023.
- [76] David E. Rumelhart, Geoffrey E. Hinton, and Ronald J. Williams. Learning representations by back-propagating errors. *Nature*, 323(6088):533–536, 1986.
- [77] Adam Paszke, Sam Gross, Francisco Massa, Adam Lerer, James Bradbury, et al. Pytorch: An imperative style, high-performance deep learning library. In *Advances in Neural Information Processing Systems 32*, pages 8024–8035. Curran Associates, Inc., 2019.
- [78] Ville Bergholm, Josh Izaac, Maria Schuld, Christian Gogolin, M Sohaib Alam, et al. PennyLane: Automatic differentiation of hybrid quantum-classical computations. *arXiv preprint arXiv:1811.04968*, 2018.